



Cu@Pt/CNT catalysts for oxygen reduction prepared by a facile two-step synthesis: Chemical vs. electrochemical leaching

Heba El-Deeb^c, Abu Bakr Ahmed Amine Nassr^a, Michael Bron^{b,*}

^a Electronic Materials Research Department, Advanced Technology and New Materials, City for Scientific Research and Technological Applications (SRTA-City), New Borg Al-Arab City 21934 Alexandria, Egypt

^b Laboratory of Industrial Chemistry I, Institute of Chemistry, Faculty of Natural Science II, Martin Luther University Halle-Wittenberg, von-Danckelmann-Platz 4, 06120 Halle (Saale), Germany

^c Fabrication Technology Research Department, Advanced Technology and New Materials Research Institute (ATNMRI), City of Scientific Research and Technological Applications (SRTA-City), New Borg Al-Arab City, 21934 Alexandria, Egypt

ARTICLE INFO

Keywords:

Oxygen reduction reaction
Electrochemical dealloying
Chemical dealloying
Platinum
Copper
Microwave-assisted synthesis
Polyol synthesis

ABSTRACT

Cu@Pt/CNT electrocatalysts were prepared by a facile two-step impregnation process. Pt nanoparticles supported on CNTs were prepared by microwave-assisted polyol reduction followed by impregnation with a copper precursor. The final catalysts were obtained by thermal alloying at different temperatures; namely 600, 800, 1000 °C. The alloying extent between Pt and Cu was found to increase significantly with the alloying temperature as revealed from XRD analysis, as does the particle size obtained from TEM. Electrochemical dealloying was performed with the three different Cu@Pt/CNT catalysts, aiming to form a core shell structure. The formation of a Pt enriched surface upon dealloying was confirmed electrochemically by cyclic voltammetry and CO stripping. The electrocatalytic activity for oxygen reduction of the electrochemically dealloyed catalysts depends on the alloying temperature where the catalyst alloyed at 800 °C showed the highest surface specific activity, which is explained in view of the high Cu content in the alloy core compared to the sample alloyed at 600 °C. Alloying at 1000 °C and chemical/electrochemical leaching leads to porous structures with high activity, albeit lower than that of the 800 °C sample. Notably these porous particles provide high activity also with a low copper content in the core. In general, the dealloyed Cu@Pt/CNT catalysts showed higher catalytic activity both in terms of surface specific activity (SSA) and mass specific activity (MSA) than their Pt/CNT counterpart.

1. Introduction

The transition from energy supply depending on fossil resources towards a production based on renewable ones requires advanced technologies able to efficiently use electricity produced from e.g. wind or solar. Splitting water into storable hydrogen and oxygen and converting the hydrogen in fuel cells to provide electricity at a later stage is intensely discussed as a very promising strategy. In this regard, polymer electrolyte membrane fuel cells (PEMFC) using hydrogen as fuel are considered suitable candidates for stationary, mobile, and portable applications [1] because of their low operating temperature, short start-up time, and relatively high power density [2]. However, these advantages are still outweighed by several obstacles that hinder the mass-market introduction of PEMFCs among which high costs are the main drawback [3,4]. One main reason for the high costs is the sluggish kinetics of

the cathodic oxygen reduction reaction (ORR) resulting in large overpotentials which limit the performance of the fuel cell [5]. Enhancement of the performance would require high loadings of the state-of-the-art cathode electrocatalyst, Pt/C, to improve the kinetics, i.e. to reduce overpotentials and thus efficiency losses. Pt is an expensive and scarce natural resource, and in consequence intensive research work has been devoted to develop active and robust electrocatalysts beyond Pt/C, i.e. reduce or even eliminate the precious metal content in the catalysts [6,7]. Alloying of Pt with non-precious metals such as 3d-transition metals is considered a promising approach to improve the ORR kinetics and reduce the financial burden of the fuel cell electrocatalysts [5,8–10]. Pt-based alloy electrocatalysts were shown to provide at least 2 times mass activity enhancement compared to that achieved by pure Pt catalyst [7], allowing for better fuel cell performance or reduced precious metal content. The enhanced activity of the Pt-based alloys

* Corresponding author.

E-mail address: michael.bron@chemie.uni-halle.de (M. Bron).

<https://doi.org/10.1016/j.jelechem.2023.117724>

Received 23 June 2023; Received in revised form 3 August 2023; Accepted 16 August 2023

Available online 18 August 2023

1572-6657/© 2023 The Author(s). Published by Elsevier B.V. This is an open access article under the CC BY license (<http://creativecommons.org/licenses/by/4.0/>).

originates from the changes occurring in the electronic (ligand effect) and geometric (strain effect) structure of the Pt lattice. As a consequence, the adsorption energies of the oxygenated intermediates are reduced, leading to lower overpotentials for the ORR [8,11–13]. One of the most active Pt-based bimetallic electrocatalysts that have been developed over the past decade is Pt-M with a core-shell structure [14,15], i.e. a Pt-M alloy core enveloped by a pure Pt shell, where M is a non-precious metal. Pt-M catalysts with core shell structure have been prepared via different routes using chemical and electrochemical methods [16]. One of the approaches for obtaining core shell structured electrocatalysts is the so-called dealloying approach: first, the PtM alloy is prepared using classical catalyst synthesis approaches followed by a dealloying process to selectively dissolve the non-precious metal component to some extent from the alloy, leaving behind a structure with an alloy in the core and a Pt-enriched shell. Chemical as well as electrochemical dealloying has been reported. Amongst other, the formed structure is determined by the interplay of dissolution of non-precious atoms versus surface diffusion of precious metal atoms [14,17,18]. Several parameters control the dealloying process and the shape of the catalysts (i.e. Pt-skin, Pt-skeleton, porous structure, etc....) such as the alloy preparation conditions, alloy composition, particle size and the used dealloying protocol (i.e. chemical or electrochemical, temperature, used acid,...) [19–21].

Although the preparation of Pt-M core-shell nanostructures using dealloying has been intensively studied, few reports on PtM supported on carbon nanotubes as a catalyst for ORR were published. Owing to their high chemical and electrochemical stability, carbon nanotubes are a promising catalyst support material for PtM as cathode catalyst in PEMFCs leading to higher activity and durability under fuel cell working conditions [22,23]. As reported earlier we used microwave-assisted polyol reduction as a novel method to prepare PtCu electrocatalysts supported on carbon nanotubes for ORR [24,25]. However, we were facing the challenge of a poor Cu ion reduction, which was also not fully resolved using a second reduction step employig NaBH_4 . In continuation of our earlier papers we report here on an attempt to optimize the actual loading of Pt and Cu supported on functionalized multiwalled carbon nanotubes to achieve the nominal ratio. Cu@Pt/CNT catalysts were prepared through a two-step impregnation synthesis approach in order to reduce metal loss caused by surfactant addition. The effect of alloying temperature of the catalysts on their structural features was studied and correlated with their catalytic activity towards oxygen reduction reaction after chemical as well as electrochemical leaching [26].

2. Experimental

2.1. Electrocatalyst preparation

A Cu@Pt/CNT catalyst (overall metal loading ca. 22 wt%, molar Pt:Cu ratio of 1:4) was prepared in two steps involving firstly the preparation of Pt/CNTs by microwave assisted polyol reduction followed by impregnation of the Pt/CNTs with a copper precursor and subsequent thermal decomposition and alloying as illustrated in Fig. 1. In detail, the as received MWCNTs (“Baytubes”, Bayer Materials Science, labelled as CNTs in the following for the sake of simplicity) were heat treated for 1 h at 800 °C under argon atmosphere to remove any volatile surface contamination. Then, the CNTs were treated with 5 M HNO_3 for 6 h at 110 °C under reflux and stirring to create adsorption sites on the inert surface of the CNTs (mostly oxygen containing groups [27]). The functionalized CNTs were washed with water for 4–6 times until the pH of the filtrate was close to 7 and finally collected by centrifugation for 20 min at 5000 rpm and dried overnight at 110 °C in air. For preparation of Pt/CNTs, 300 mg of the functionalized CNTs were homogenously dispersed by magnetic stirring for 30 min in 80 ml ethylene glycol (EG) which acts as a solvent and reducing agent (heating up ethylene glycol solution generates acetaldehyde [28] or glycolaldehyde [29] which in turn act as a reductant). Thereafter, 10 ml 0.02297 M $\text{H}_2\text{PtCl}_6/\text{EG}$ solution was added dropwise to the CNTs/EG mixture followed by addition of 20 ml PVP/EG solution (Polyvinylpyrrolidone, $M = 10000$) with a metal to PVP ratio of 1:5 (based on monomer units of PVP). PVP was added here as a stabilizer to ensure the homogenous dispersion of the Pt nanoparticles on the CNTs and to avoid metal agglomeration. The reaction mixture was left under continuous stirring for 3 h followed by sonication for 30 min before being subjected to a microwave irradiation at 700 W in a pulsed mode with t_{on} 150 s and t_{off} 60 s with a total irradiation time of 10 min (see supplementary information, Figure S11 for the temperature profile during synthesis). Afterwards the reaction mixture was kept under stirring overnight followed by addition of 100 ml of absolute ethanol to sediment the particles. After 1 h the Pt/CNT catalyst was washed several times with water and dried overnight at 100 °C. The microwave step in a typical synthesis should produce 13 wt % of nominal Pt loading however, the loading established from TGA analysis (see below) was ca. 10.6 wt%, which was expected based on our earlier reports [24,25]. The as-prepared Pt/CNT catalyst was heat treated in a horizontal tube furnace at 185 °C under ambient atmosphere for 5 h to remove any remaining PVP [30,31]; this catalyst is labelled Pt/CNTs_{HT}. For the second impregnation step, 200 mg of Pt/CNTs_{HT} were dispersed in 80 ml absolute ethanol for 30 min before dropwise adding 20 ml of 0.02157 M $\text{CuSO}_4/\text{EtOH}$ solution followed by stirring at

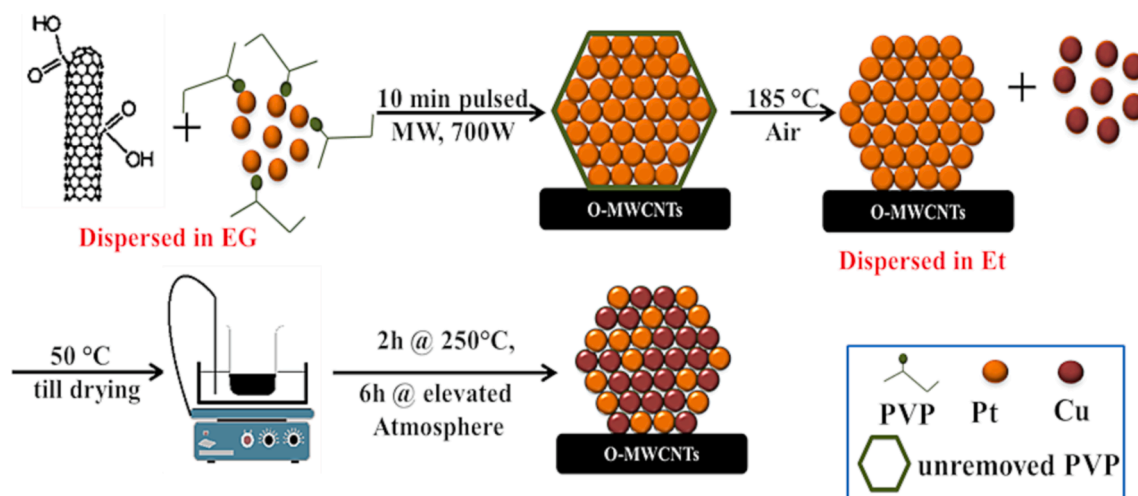


Fig. 1. Schematic illustration for the Cu@Pt/CNTs_x catalyst preparation.

room temperature overnight. Afterwards the catalyst suspension was kept at 40 °C in a water bath for EtOH evaporation until a thick black slurry was obtained, followed by drying in an oven overnight at 60 °C and grinding in a mortar. To obtain the final Cu@Pt/CNT catalyst, the following protocol has been applied for alloying: first, the catalyst was heat treated under flowing H₂/Ar stream (10 % H₂) with a heating rate of 10 °C min⁻¹ for 2 h at 250 °C to initiate the decomposition of the copper precursor through releasing the hydrate water molecules [32–34], followed by annealing of the catalyst for 6 h at elevated temperatures of 600, 800, and 1000 °C in the same atmosphere for final precursor decomposition and alloying. The alloyed catalysts were cooled down to room temperature and are labelled Cu@Pt/CNTs_x, where *x* refers to the annealing temperature. The annealed catalysts in form of a thin layer electrode were subjected to an electrochemical dealloying step by cycling the electrode in acidic solution (0.1 M HClO₄) for 200 potential cycles at a scan rate of 200 mV/s. These electrochemical stress conditions force the selective dissolution of the (surface) metal constituents with less-noble character (here: Cu) leaving behind a Pt enriched surface or particle. Alternatively, the dealloying process was carried out chemically in acidic solution for a specific time to distinguish the two methods of dealloying and their effect on the catalyst activity towards ORR. The Cu@Pt/CNTs₁₀₀₀ catalyst was selected for this differentiation due to its higher alloying degree in comparison with the catalysts annealed at lower temperatures (i.e. 600 °C and 800 °C; see results). The chemical dealloying of the Cu@Pt/CNTs₁₀₀₀ catalyst has been carried out for 1 h and 4 h in 1 M HClO₄.

2.2. Catalyst characterization

2.2.1. Structural characterization

X-ray diffraction (XRD) patterns of the various catalysts were obtained on a Bruker AXS D8 advanced X-ray diffractometer with a CuK_α X-ray source (0.15406 nm) in the 2θ range of 20–80° at a scan rate of 2° min⁻¹. The catalyst morphology was investigated with a LEO 912 transmission electron microscope (TEM) operating at an acceleration voltage of 120 keV. Particle size distributions were determined using the line242e software by determining the particle sizes of ca. 200 particles for each catalyst. The metal loadings of the catalysts were established by thermogravimetric analysis (TGA) performed on a NETZSCH, STA 449 F1 Jupiter thermobalance with a heating rate of 10 K min⁻¹ in a 25 % O₂ in Ar atmosphere with a flow rate of 20 ml min⁻¹ up to a temperature of 1000 °C. Under these conditions the carbon is completely oxidised. Additionally, the Pt and Cu contents of the catalysts were determined with inductively coupled plasma–optical emission spectroscopy (ICP-OES) using an Ultima 2, HORIBA Jobin Yvon, after digestion in aqua regia using a microwave reactor.

2.2.2. Electrochemical characterization

The electrochemical measurements were conducted in a one compartment three electrode electrochemical cell containing 0.1 M HClO₄ as electrolyte solution at room temperature. The working electrode was a catalyst coated glassy carbon (GC) substrate 4 mm in diameter inserted into a Teflon holder. The reference electrode was a reversible hydrogen electrode (RHE) in 0.1 M HClO₄ and all potentials in this work are reported against this electrode. A Pt mesh was used as counter electrode. The thin layer catalyst electrode was prepared by mixing 2.5 mg of the catalyst with 315 μl isopropanol and 35 μl 5 wt% Nafion solution as a binder. The catalyst ink was sonicated and stirred for 3 h each, and aged overnight before casting a 10 μl aliquot onto the surface of a previously polished and cleaned GC substrate. Slow drying in isopropanol atmosphere resulted in a smooth surface without any cracks. The electrochemical cell was connected to an Autolab potentiostat/galvanostat (PGSTAT128N, Metrohm) controlled by the NOVA 1.8 software.

Prior to determining the electrocatalytic activity, an electrochemical dealloying step of the alloyed catalysts Cu@Pt/CNTs_x was performed in

N₂-deaerated 0.1 M HClO₄ electrolyte solution keeping N₂ flowing over the solution during the measurements. The electrochemical dealloying protocol was initiated by 3 CVs in the potential range between 0.05 and 1.2 V with a scan rate of 100 mV s⁻¹ to acquire the initial profiles of Cu dissolution. Then the actual dealloying was carried out on the catalyst-coated electrode using 200 potential cycles with a scan rate of 200 mV s⁻¹ in the same potential range. Thereafter, the dealloying protocol concludes with 3 CVs in the potential range between 0.05 and 1.1 V and scan rate of 100 mV s⁻¹ and the last CV was used to estimate the electrochemically active surface area (ECSA_{Hupd}) of the catalysts. The pre-treatment of the Pt/CNT catalyst and the chemically dealloyed samples to establish the electrocatalytic activity consists of 20 CVs in the potential range between 0.05 and 1.1 V at 100 mV/s in N₂ deaerated 0.1 M HClO₄ electrolyte and the final CV was used to estimate the electrochemical surface area. The electrochemical active surface areas were also determined by carbon monoxide stripping (ECSA_{CO}) according to a previously reported procedure [24,25].

Subsequently, linear sweep voltammograms using a rotating disc electrode (RDE) were recorded to evaluate the electrocatalytic activity and the kinetic parameters for the oxygen reduction reaction (ORR) in oxygen-saturated 0.1 M HClO₄. The potential was swept positively from 0.05 to 1.1 V vs. RHE with a scan rate of 5 mV s⁻¹ at different rotation speeds of 400, 900 and 1600 revolutions per minute (rpm). An O₂ flow was kept passing over the surface of the solution during all measurements. The ORR currents of the catalysts were corrected for the capacitive currents by subtracting the background currents of the sweeps recorded in N₂-saturated electrolyte from those measured in O₂-saturated electrolyte. Moreover, the ORR current densities were corrected for mass transport effects to obtain the kinetic current densities using the Koutecky-Levich equation (see section 3). The mass and surface specific activities of the catalysts were established at 0.85 and 0.9 V vs. RHE at a rotation rate of 900 rpm for comparison.

3. Results and discussion

3.1. Catalyst characterization

The XRD patterns of the prepared as well as of reference catalysts are displayed in Fig. 2 and organized in three sections for comparison. All XRD patterns display a broad diffraction peak at 2θ ca. 25° corresponding to the diffraction at the graphene layers of CNTs beside three main peaks at 2θ values of ca. 39.7°, 46° and 67.6° characteristic for the 111, 002 and 022 planes of Pt with a face centered cubic structure (FCC) [35,36]. The bottom layer in Fig. 2 compares the diffraction patterns of the Pt/CNT catalysts. Noticeably, the diffraction peaks of Pt/CNTs_{HT} are found at slightly higher 2θ values compared to those of Pt/CNTs, where the former are identical to the diffraction peak of Pt/C (ETEK) [25]. Thermogravimetric investigations (Fig. 3) indicate a slight weight loss during heat treatment in oxygen-containing atmosphere below 200 °C as well as a second weight loss at ca. 300 °C, followed by a third weight loss at temperatures above 400 °C attributed to the oxidative decomposition of CNTs. The first peak is, based on literature reports, attributed to the decomposition of PVP [30,31], while the second peak may stem from the decomposition of instable surface functional groups [27]. As we do not assume that the removal of PVP from the Pt surface may have a strong influence on the XRD patterns, likely the above-mentioned peak shifts are due to the presence of incomplete reduction products formed during catalyst synthesis, which then decompose during heat treatment at 185 °C.

The XRD diffraction patterns in the middle section visualize the influence of the annealing temperature on the structure of the Cu@Pt/CNT catalysts. Distinct changes can be observed with increasing annealing temperature. Starting from 600 °C, the diffraction peaks of the annealed catalysts (Cu@Pt/CNTs_x) attributed to Pt (e.g., Pt 111 at ca. 40°) are shifted to higher 2θ values (comp. also Table 1). This decrease in the lattice parameter of the unit cell indicates alloy formation between Pt

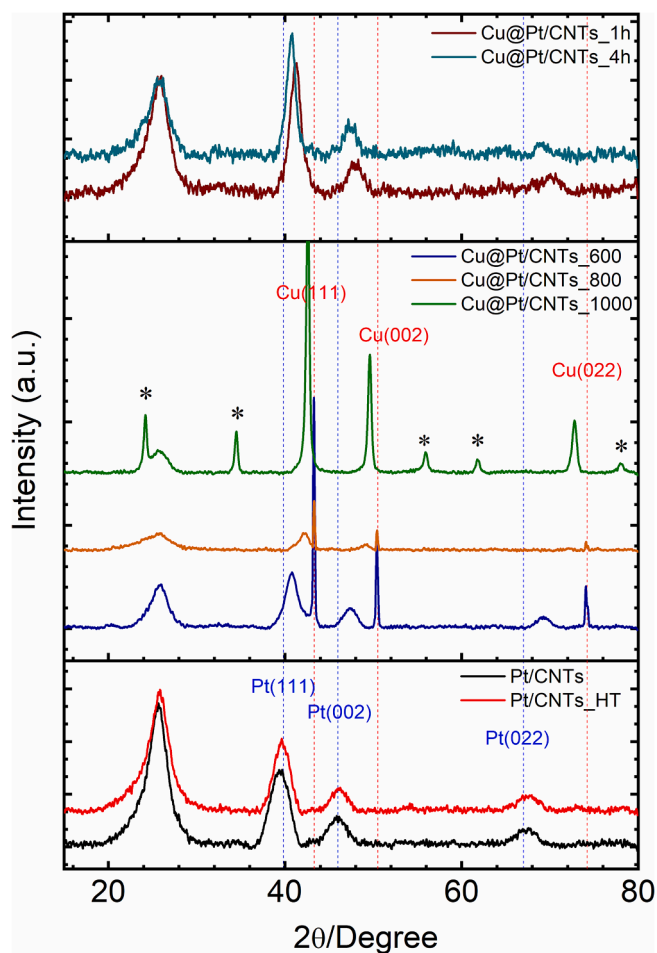


Fig. 2. XRD patterns of all catalysts: as prepared (bottom), after alloying (middle) and after chemical leaching (top) Peaks marked with a * are characteristic to the PtCu superlattice planes. Dashed lines: position of relevant reflexes from databases. Blue: Pt, COD 9008480; red: Cu, COD 9008468.

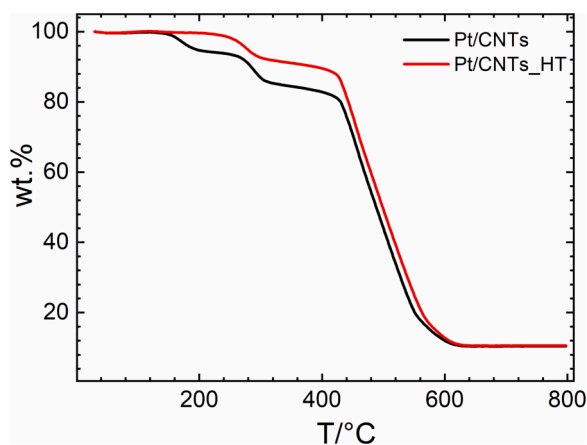


Fig. 3. TGA curves of Pt/CNTs and Pt/CNTs_{HT}. 25 % O₂ in Ar, 10 K min⁻¹.

and Cu by incorporation of Cu into the Pt lattice. However, additional diffraction peaks are observed in the Cu@Pt/CNTs₆₀₀ and Cu@Pt/CNTs₈₀₀ XRD patterns at 2θ ca. 43° , 51° and 74° . These peaks correspond to the 111, 002 and 022 planes of pure Cu [37,38], indicating that after annealing at 600 °C and 800 °C, two phases coexist, where one is the alloy, and the other a pure copper phase, and that these temperatures are insufficient to achieve well-alloyed catalysts. Reflexes of pure copper

are missing in the diffractogram of Cu@Pt/CNTs₁₀₀₀, indicating complete alloying. Noteworthy are the four diffraction peaks at $2\theta = 24.1^\circ$, 34.4° , 55.7° and 61.7° found in the sample annealed at 1000 °C (marked with *) that are characteristic to the PtCu superlattice planes [39], indicating a highly ordered structure.

Using Vegard's law, the Pt and Cu content of the alloys was calculated from the 111 diffraction. In Table 1, these values are displayed together with those determined by ICP-OES, which are related to both alloyed and un-alloyed copper. As expected the Cu content of the alloy increases with increasing alloying temperature, nearly reaching the nominal one at 1000 °C, while the ICP-derived value nearly yields the nominal loading for each annealing temperature. However, annealing comes along with an increase in the particle size. Crystallite as well as particle sizes for all catalysts determined from XRD using the Scherrer equation as well as from TEM (for TEM images and particle size distributions see supplementary information, Figure SI2a and b) are summarized in Table 1, clearly demonstrating particle growth by annealing. It seems somewhat implausible that the crystallite sizes are larger than the particle sizes. We assume that it is not appropriate to simply use 0.9 as a shape factor in the Scherrer equation, as it is usually done. A smaller shape factor would lead to smaller particle sizes, which would probably fit better to the TEM results. Furthermore, it is important to note that the samples are rather heterogeneous in their size distribution. While in TEM the smaller particles clearly contribute to the particle size distribution, in XRD the influence of the larger particles should be larger. However, the tendency of particle growth is clearly visible.

The chemical dealloying of the Cu@Pt/CNTs₁₀₀₀ catalyst for 1 h and 4 h in 1 M HClO₄ leads to broadening of the diffraction peaks and a shift to lower 2θ values, beside disappearance of the diffraction peaks corresponding to the ordered intermetallic structure as presented in the upper section in Fig. 2. The 2θ shift can be easily explained by loss of Cu from the Cu lattice, leaving behind a Pt-rich alloy. Respective compositions established from XRD and ICP-OES are displayed in Table 1 and fit well to each other. It is important to note, that the superstructure is completely lost during chemical dealloying. Similar findings have been reported by us for carbon-black-supported PtCu catalysts prepared in a different way [40] and indicate that chemical leaching penetrates deep into the core of the material. Furthermore, the strong decrease of crystallite size concomitant with only a slight decrease in particle size demonstrates that severe restructuring of the particles occurs, leading behind a much less ordered structure.

The metal loadings of all catalysts were determined by ICP-OES as well as by thermogravimetric analysis (TGA, see Supplementary Information Figure SI3) and are listed in Table 2. The nominal metal loading of the as-prepared Cu@Pt/CNT catalyst was controlled to be ca. 22 %, while that of Pt/CNTs was 13 % (yielding a Pt:Cu ratio of 1:4; see experimental). However, the annealed catalysts, as specified from TGA and ICP-OES analysis, exhibit an increase in the metal loading over the nominal one as the annealing temperature increases from 600 °C to 1000 °C, which could be due to the removal of almost all the oxygenated groups attached to the CNT surface during the annealing and decomposition/volatilization of parts of the carbon nanotubes [41]. Moreover, the TGA analysis of the chemically dealloyed catalysts Cu@Pt/CNTs_{1h} and Cu@Pt/CNTs_{4h} in 1 M HClO₄ reveals a decrease in the metal loading from 24.5 wt% to 14.5 wt% when compared with the counterpart catalyst, Cu@Pt/CNTs₁₀₀₀. Such drastic decrease in the metal content is attributed to the severe drop in the Cu content (i.e. Cu dissolution) as demonstrated from ICP-OES data in Table 2, which in turn leads to a slight relative increase in Pt wt.%. Extending the chemical dealloying time from 1 h to 4 h decreases the Pt and Cu loading, with the latter being at less than 10 % of the initial value. It is clear that such a drastic loss in Cu content must lead to significant changes in the catalyst structure, as analyzed below with TEM.

TEM images of all catalysts with the exception of the chemically dealloyed ones are displayed in the supplementary information in Figure SI2a. Generally, the nanoparticles of the catalysts are well-

Table 1

Average particle sizes established from TEM, XRD parameters, Pt:Cu ratio determined from the XRD and ICP-OES.

Catalyst	Particle size(nm) ^a	Crystallite size(nm) ^b	Inter- planar distance (Å) ^c	Lattice constant (Å) ^d	2θ ₁₁₁	Pt:Cu _{XRD} At. %	Pt:Cu _{ICP} At. %
Pt/CNTs	2.76	3.11	2.28	3.959	39.38	–	–
Pt/CNTs _{HT}	2.83	3.76	2.27	3.936	39.62	–	–
Cu@Pt/CNTs ₆₀₀	3.53	4.57	2.21	3.828	40.79	Pt ₆₉ Cu ₃₁	Pt ₁₇ Cu ₈₃
Cu@Pt/CNTs ₈₀₀	5.81	6.31	2.14	3.708	42.16	Pt ₃₀ Cu ₇₀	Pt ₂₀ Cu ₈₀
Cu@Pt/CNTs ₁₀₀₀	12.52	17.70	2.12	3.674	42.58	Pt ₁₉ Cu ₈₁	Pt ₁₆ Cu ₈₄
Cu@Pt/CNTs _{1h}	11.54	5.31	2.19	3.792	41.19	Pt ₅₇ Cu ₄₃	Pt ₆₁ Cu ₃₉
Cu@Pt/CNTs _{4h}	10.57	7.03	2.21	3.837	40.69	Pt ₇₂ Cu ₂₈	Pt ₇₀ Cu ₃₀

^a mean particle size of ca. 200 nanoparticles analyzed from TEM images.^b crystallite size established from the FWHM of XRD diffraction peaks,.^c interplanar distance established from Bragg's law ($\lambda = 2 \sin\theta$),^d lattice parameter according to the 111 peak ($a = d\sqrt{h^2 + k^2 + l^2}$).**Table 2**

Metal loading (wt.%) as estimated from ICP-OES and compared with the total metal loading from TGA analysis.

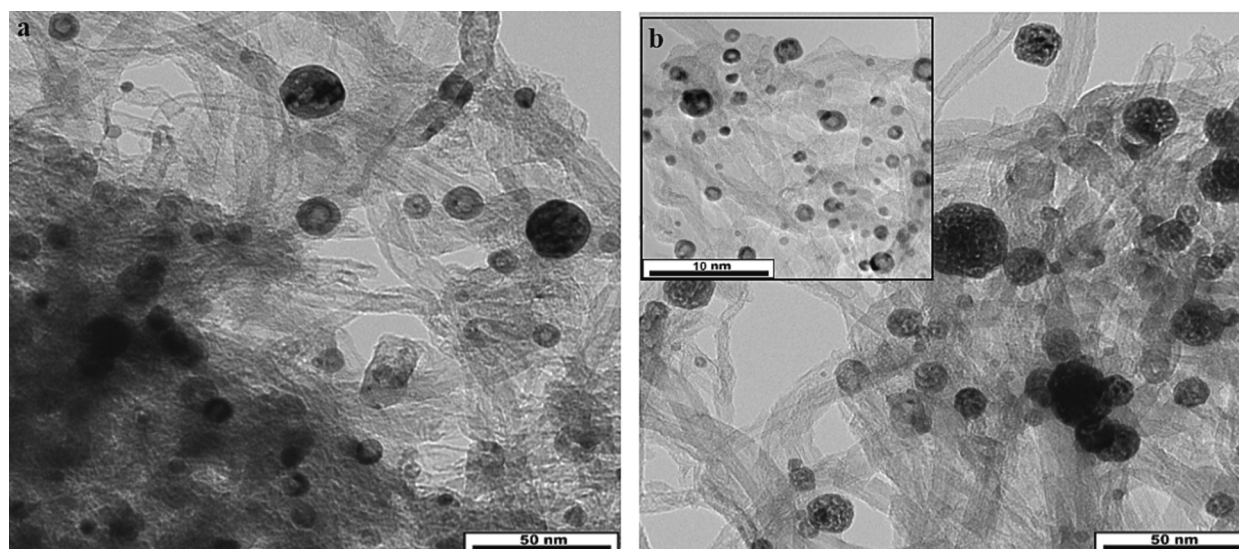
Catalyst	Pt wt. %	Cu wt. %	Total _{ICP} wt. %	Total _{TGA} wt. %
Pt/CNTs	10.6	–	–	10.6
Pt/CNTs _{HT}	10.5	–	–	10.5
Cu@Pt/CNTs ₆₀₀	7.8	12.2	19.9	23.9
Cu@Pt/CNTs ₈₀₀	10.1	13.1	23.2	23.9
Cu@Pt/CNTs ₁₀₀₀	10.2	17.6	27.8	24.5
Cu@Pt/CNTs _{1h}	13.3	2.8	16.1	14.5
Cu@Pt/CNTs _{4h}	11.4	1.6	13.0	14.5

dispersed on the catalyst support and have a narrow particle size distribution and compact appearance. Average particle sizes are listed in Table 1 and were discussed already together with the XRD results.

A more detailed look will be taken at the TEM images of the chemically dealloyed catalysts Cu@Pt/CNTs_{1h} and Cu@Pt/CNTs_{4h}, which are shown in Fig. 4a and b. As expected, the TEM images have significantly changed compared to those of the initial catalyst particles, which appear to be compact (cf. supporting information Figure SI2a, image e). After 1 h of chemical dealloying, obviously core-shell particles or even particles with hollow structure are formed. Prolonged dealloying for 4 h results in a highly porous structure as visible in Fig. 4b. Furthermore, higher resolution images (inset in Fig. 4b) demonstrate the formation of core-shell or hollow structures as well, in line with the extended loss of Cu and a leaching process penetrating deep into the particle. During the

chemical dealloying of the Pt-based alloy, it is expected that the less noble metal (i.e. Cu in this case) is selectively dissolved from the outer regions of the alloy, while the less reactive metal (i.e. Pt) tends to restructure and possibly forms a passivating layer on the surface blocking further dissolution. However, according to [42,43] this passivation layer is not entirely stable in the harsh corrosive conditions and starts to exfoliate allowing dissolution to proceed into considerable depth of the larger particles causing the formation of a three dimensional nanoporous structure. Generally, it seems that Cu@Pt/CNT particles with smaller size (<15 nm) tend to form a core-shell or hollow structure while the Cu@Pt/CNT particles larger than 15 nm tend to form a highly nanoporous structure, similar result have been found by Oezaslan et al. [20] and Wang et al. [44]. It can be assumed that during prolonged leaching parts of the Pt from the Pt-skeleton/open structure that formed during the chemical dealloying process detach (see decrease in Pt content, Table 2), allowing the electrolyte to enter also the inner layers of the catalysts leading to further Cu dissolution. With longer dealloying time the Pt-skeleton might partly collapse or restructure, which could explain the increase in crystallite size found in XRD (see Table 1).

It should, however, be mentioned that analysis of the largest particles with EDX-STEM (Figure SI4 in the supplementary information) demonstrates, that these particles still have a gradient in composition with a pure Pt shell (lower images in Figure SI4) and an alloyed core with a composition of Pt₂₅Cu₇₅ (upper images). Probably a prolonged dealloying time would be necessary to further remove copper from the particle core.

**Fig. 4.** TEM images of the chemically dealloyed catalysts: a) Cu@Pt/CNTs_{1h}, b) Cu@Pt/CNTs_{4h}; inset: HRTEM of Cu@Pt/CNTs_{4h} catalyst.

3.2. Electrochemistry

Fig. 5 shows the initial cyclic voltammograms (CVs) of the catalysts Cu@Pt/CNTs₆₀₀₋₁₀₀₀ recorded in N₂-saturated 0.1 M HClO₄ solution with a scan rate of 100 mV s⁻¹. No features of a Pt containing surface, i.e. hydrogen adsorption/desorption peaks (H_{UPD}) in the potential range of 0.05 V to 0.3 V, the double layer region, or the Pt oxide formation/reduction are visible for the sample annealed at 600 °C. Instead, a broad anodic Faradic peak in the potential range between 0.3 V and 0.85 V can be seen, consistent with Cu leaching from an alloy with a high Cu surface content and remainders of unalloyed Cu. Furthermore, increasing the annealing temperature leads to a gradual reduction in the Cu stripping peak height, in line with the reduction of the amount of the unalloyed Cu found by XRD. In contrast, the first CVs of the Pt/CNTs, Pt/CNTs_{HT}, Cu@Pt/CNTs_{1h}, and Cu@Pt/CNTs_{4h} catalysts do not exhibit any features characteristic for a Cu-rich surface but show more or less pronounced Pt features (Figure S15, supplementary information).

Fig. 6a-c illustrate the final cyclic voltammograms of the different catalysts under investigation recorded in N₂-saturated 0.1 M HClO₄ solution with a scan rate of 100 mV s⁻¹. The CVs for the Cu@Pt/CNTs_x samples were recorded after the electrochemical dealloying (200 CVs at 200 mV s⁻¹), while the final CVs for the Pt/CNT catalysts and the chemically dealloyed catalysts were recorded after electrochemical cleaning/activation. Basically, the final CVs of all catalysts behave like those of Pt surfaces nevertheless with some differences. The CV of the heat-treated Pt catalyst, Pt/CNTs_{HT}, shows a more intense H_{upd} than the as-prepared Pt/CNT catalyst as shown in Fig. 6a, resulting in a ca. 1.25 times higher ECSA_{Hupd} (Table 3). However, the oxide formation/reduction peaks are still weakly expressed. This difference in the ECSA_{Hupd} could be assigned to a blocking of ca. 25 % of the active surface sites of the Pt/CNTs catalyst by unremoved PVP traces, as mentioned before. Chung et al. [45] reported that the hydrogen underpotential deposition region of a commercially available Pt/C catalyst treated with oleylamine as a surfactant displays a significant decrease in the ECSA compared to the untreated Pt/C catalyst; they claim that the surfactant effectively adsorbed on the Pt active sites and blocked about 70 % of the surface. Safo et al. [46] studied the effect of different capping agents on the ORR activity and claimed that the ECSA of the catalysts treated with PVP and oleylamine increases in the order of: PVP-capped Pt < oleylamine-capped Pt < Pt/C. Further, they demonstrated that even after washing, the capping agents remain at the particles surface and block the catalytically active sites for the ORR.

The final cyclic voltammograms of the annealed catalysts Cu@Pt/CNTs₆₀₀₋₁₀₀₀ after 200 dealloying cycles exhibit a dramatic transformation from a Cu-rich alloy surface to a Pt-like surface as shown in Fig. 6b compared to Fig. 5. The transformation from a Cu-segregated

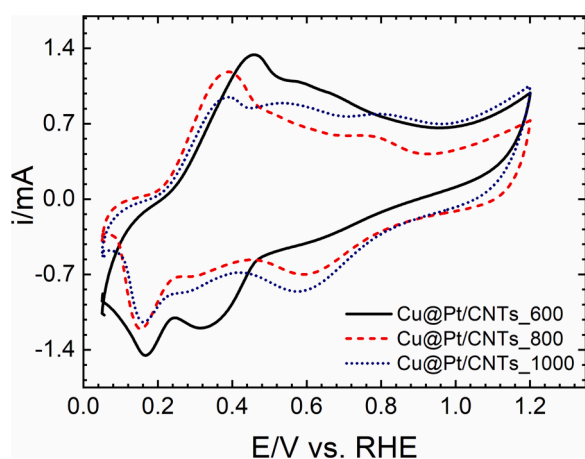


Fig. 5. Cyclic voltammograms of Cu@Pt/CNTs_x catalysts conducted in N₂ saturated 0.1 M HClO₄ solution (sweep rate of 100 mV s⁻¹, first CV).

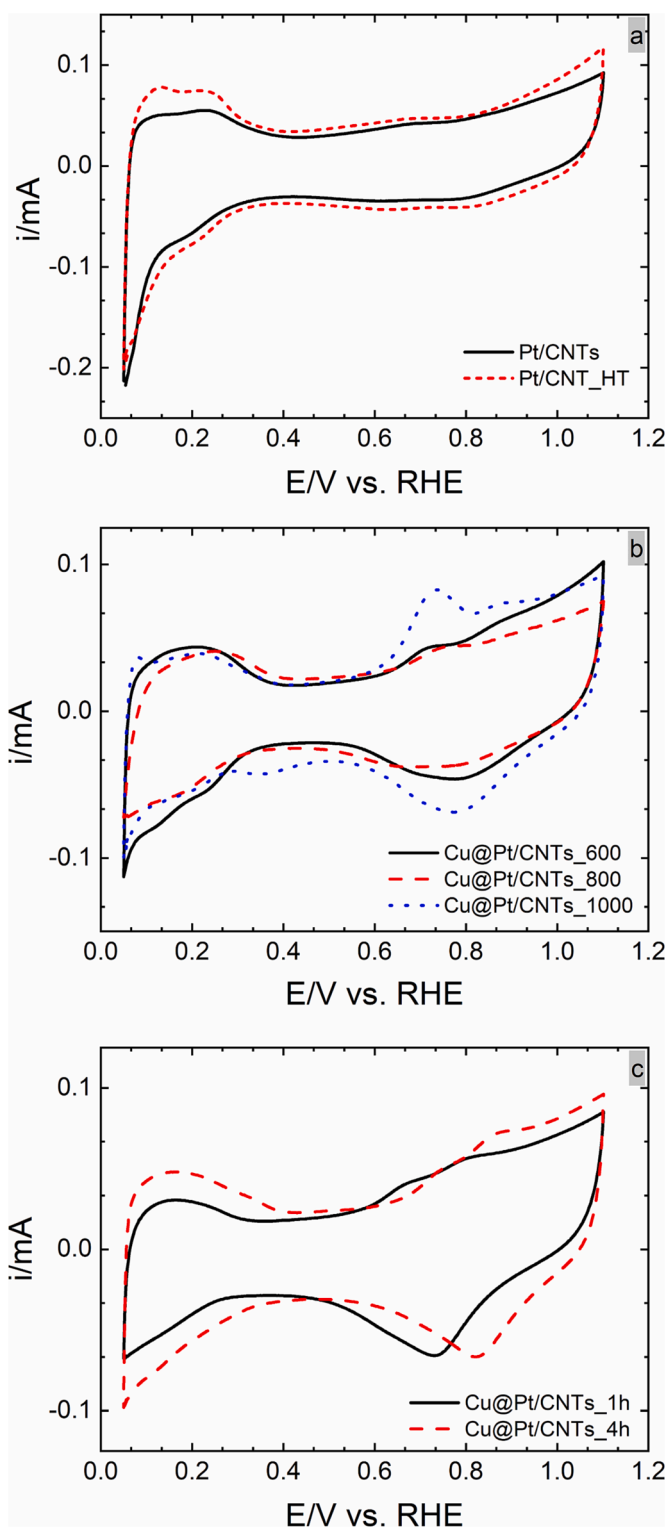


Fig. 6. Cyclic voltammograms of a) Pt/CNT catalysts, b) the electrochemically dealloyed Cu@Pt/CNT catalysts and c) chemically dealloyed Cu@Pt/CNTs₁₀₀₀ catalyst (in 0.1 M HClO₄, 100 mV s⁻¹).

surface to a Pt-like CV profile for Cu@Pt/CNTs₆₀₀ is shown in Figure S16 in the supplementary information. Generally, the electrochemically active surface areas (ECSA) of the catalysts were evaluated from the charge associated with the H_{upd} stripping (Q_H), namely ECSA_{Hupd}. To calculate the ECSA_{Hupd}, Q_H was normalized using a surface area specific charge of a one-electron transfer, i.e. 210 μC cm⁻² for

Table 3

Q_H values, Q_{CO} values, the ECSA obtained from H_{upd} and CO stripping, and the $Q_{CO}/2Q_H$ ratio of the Pt/CNTs, Pt/CNTs_{HT} and the electro/chemically dealloyed catalysts; the charges were normalized to the electrode geometric area.

Electro (Chemical) dealloyed catalysts	$Q_H/\mu\text{C cm}^{-2}$	$Q_{CO}/\mu\text{C cm}^{-2}$	$\text{ECSA}_{H_{upd}}/\text{m}^2 \text{ g}_{Pt}^{-1}$	$\text{ECSA}_{CO}/\text{m}^2 \text{ g}_{Pt}^{-1}$	$Q_{CO}/2Q_H$
Pt/CNTs	86.88	185.36	68.80	73.40	1.06
Pt/CNTs _{HT}	112.80	237.6	88.51	93.22	1.05
Cu@Pt/CNTs ₆₀₀	107.44	307.12	57.78	82.59	1.42
Cu@Pt/CNTs ₈₀₀	64.24	168.88	26.45	34.77	1.31
Cu@Pt/CNTs ₁₀₀₀	59.60	161.76	24.35	33.05	1.35
Cu@Pt/CNTs _{1h}	36.80	107.60	23.04	33.70	1.46
Cu@Pt/CNTs _{4h}	51.36	140.01	37.45	51.12	1.36

hydrogen adsorption on a Pt surface [47]. The $\text{ECSA}_{H_{upd}}$ for all catalysts was calculated and is depicted in Table 3. Noticeable, the adsorbed hydrogen amounts, H_{upd} , of the electrochemically dealloyed catalysts dramatically decrease as the annealing temperature increases from 600 °C to 1000 °C. This decrease in the $\text{ECSA}_{H_{upd}}$ of the Cu@Pt/CNTs₈₀₀ and Cu@Pt/CNTs₁₀₀₀ catalysts by 61.9 % and 64.9 % respectively relative to Cu@Pt/CNTs₆₀₀ could be attributed to the increase in the mean particle size of the catalysts as evidenced from TEM analysis (Table 1, Figure S12) for the catalysts annealed at higher temperature.

Some remarks shall also be given on the CVs of the chemically dealloyed catalysts shown in Fig. 6c. The catalyst Cu@Pt/CNTs_{4h} shows a higher H_{upd} resulting in a ca. 1.5 times higher $\text{ECSA}_{H_{upd}}$ than that of the Cu@Pt/CNTs_{1h} although the former has only a slightly smaller mean particle size and higher Pt content. Such ECSA enhancement could be attributed to the formation of a three-dimensional nanoporous structure as demonstrated by our TEM results. Furthermore, a positive shift of ca. 95 mV vs. RHE is observed in the peak potential of the oxide reduction peak of the Cu@Pt/CNTs_{4h} catalyst when compared with the Cu@Pt/CNTs_{1h} catalyst and the other samples.

It was suggested [48] that the electrochemical surface area of Pt-based catalysts should be confirmed using CO stripping to avoid the underestimation of the ECSA owing to the possible suppression of H_{upd} adsorption, which would lead to an overestimation of the specific activity. Fig. 7 summarizes the representative CO stripping voltammograms (1st and 2nd cycle) for all catalysts under investigation. Apparently, prior to the electro-oxidation of the adsorbed CO monolayer from the catalyst surface the H_{upd} is completely suppressed as result of surface site blocking by CO, while after CO electro-oxidation the peaks associated with H_{upd} emerge again. Furthermore, the onset potential of CO oxidation on the Cu@Pt/CNTs_x catalysts whatever they are chemically or electrochemically dealloyed is 60 to 180 mV lower than that on the pure Pt catalysts. This negative shift in CO oxidation potential is attributed to the weaker interaction between the Pt surface atoms and CO due to their modified electronic properties, probably as a result of lattice strain. A pronounced dependency is noticed where with increasing mean particle size the CO stripping peak potential shifts negatively (see Table 1 for particle sizes). This size dependency of CO monolayer electro-oxidation was also observed in previous investigations [49,50]. From CO stripping the electrochemically active surface area (ECSA_{CO}), as listed in Table 3, was estimated by normalizing the measured charge (Q_{CO}) using the surface area specific charge of an ideal two-electron transfer ($420 \mu\text{C cm}^{-2}$), assuming the oxidation of one CO molecule to CO_2 per Pt atom. One important finding is that dealloyed catalysts are found to exhibit over 30 % lower $\text{ECSA}_{H_{upd}}$ relative to ECSA_{CO} , while no significant discrepancy has been recorded between the electrochemically active

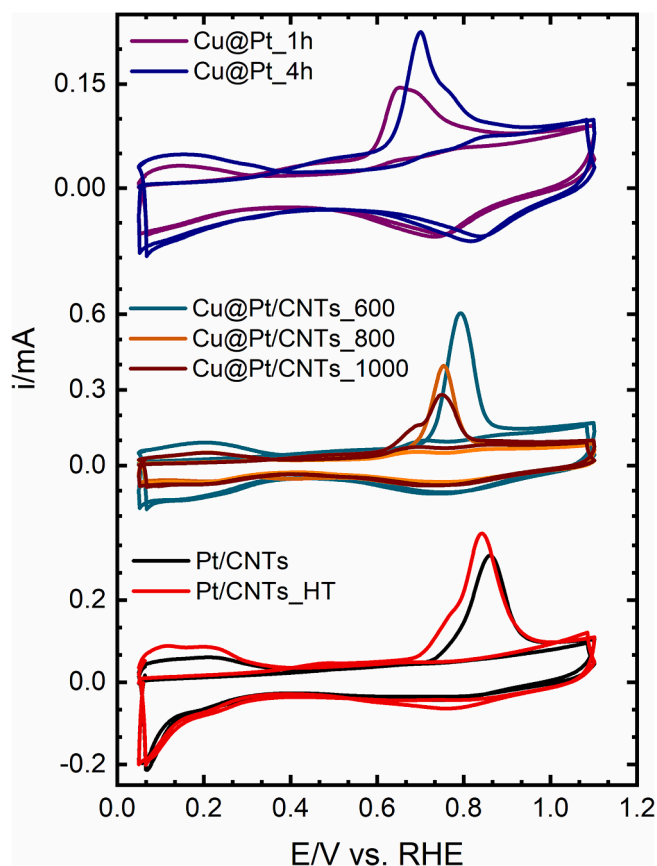


Fig. 7. Representative CO stripping voltammograms of the Pt catalysts and the electrochemically/chemically dealloyed Cu@Pt/CNT catalysts in 0.1 M HClO_4 (20 mV/s scan rate).

surface areas estimated from the H_{upd} and CO stripping for the Pt/CNTs and Pt/CNTs_{HT} catalysts. Vliet et al. [51] and Wang et al. [52] demonstrated that the surface coverage of H_{upd} on a Pt-skin surface is about half of that found on pure Pt (1 1 1), whilst the surface coverage of a saturated CO monolayer is similar on both surfaces. It is reasoned that the adsorption of H_{upd} on a Pt surface layer formed after dissolution of the d element of an alloy is greatly affected (i.e. suppressed H_{upd} behavior) [12,53] due to the altered electronic properties, while CO adsorption is not affected due to the strong Pt-CO interaction [11]. In this regard, this discrepancy in the ECSA obtained from H_{upd} vs. CO was suggested to prove the formation of a Pt-skin surface layer over Pt-bimetallic systems [52,53]. As mentioned above, the ratio between the surface charges $Q_{CO}/2Q_{H_{upd}}$ is close to unity in case of pure Pt systems, while the $Q_{CO}/2Q_H$ ratio obtained for Pt skin surfaces is always greater than unity.

The activity of the catalysts towards ORR was studied using LSV with an RDE at different rotation speeds in O_2 -saturated 0.1 M HClO_4 electrolyte solution between 0.05 and 1.1 V vs. RHE with a scan rate of 5 mV s^{-1} . The ORR polarization curves of all catalysts are shown in Figure S17 in the supplementary information, showing the three well known potential regimes, namely by sweeping positively the well-defined diffusion-limited regime (E less than 0.75), the mixed kinetic-diffusion controlled regime, and the kinetically control regime (E greater than 1.0). To determine the ORR kinetics, the ORR curves at different rotation speeds were analyzed using the Koutecky–Levich (K–L) equation:

$$\frac{1}{j} = \frac{1}{j_k} + \frac{1}{j_d} = \frac{1}{j_k} + \frac{1}{B\omega^{1/2}}$$

Where j is the measured current density, j_k is the kinetic current density, j_d is the diffusion-limited current density, ω is the angular

frequency of rotation ($2\pi/60 \times f$, f : rotation in rpm), and B is the Levich constant.

As a first estimation, the half wave potential ($E_{1/2}$) can be used to compare the catalytic activity for a set of catalysts, which is defined as the potential at which the current density reaches half of its diffusion-limited value. $E_{1/2}$ for all catalysts were determined from the ORR polarization curve at 900 rpm and are listed in Table 4. $E_{1/2}$ exhibits a considerable shift to higher potentials (i.e., higher ORR activity) in the sequence Pt/CNTs < Pt/CNTs_{HT} < Cu@Pt/CNTs_{1h} < Cu@Pt/CNTs_{4h} < Cu@Pt/CNTs₁₀₀₀ < Cu@Pt/CNTs₈₀₀ < Cu@Pt/CNTs₆₀₀. For a more precise activity evaluation, specific kinetic currents (mass specific activity, i.e. activity related to Pt loading, and surface specific activity) were determined based on the kinetic current densities (j_k) at 0.85 V and 0.9 V obtained from Tafel plots as displayed in Fig. 8 using the known catalyst loadings or the ECSA determined by CO stripping. The results are summarized in Table 4. A significant improvement in the mass and surface specific activities of the chemically or electrochemically dealloyed catalysts relative to pure Pt catalysts is observed, which shall be discussed in light of the above structural characterization in the following.

4. Discussion

The enhanced activity of the electrochemically dealloyed catalysts compared to their pure Pt counterpart is typically attributed to the formation of a Pt-rich surface surrounding a Cu-rich PtCu alloy core in literature [16,54]. As discussed before, this may give rise to a surface lattice strain resulting in a downshift in the d-band center which weakens the interaction between the oxygen containing species and Pt surface during the ORR [54]. The absence of any Cu features in the CVs of our catalysts alloyed at 600, 800 and 1000 °C after electrochemical leaching may indicate, that this structural model does also apply in our case. However, in literature it has also been shown that for larger alloy particles porous structures may form instead of core-shell systems as a result of electrochemical leaching [20]. Indeed, the average particle size of the alloyed particles increases from 3.5 nm to 12.5 nm in our case, while the Pt:Cu ratio in the alloy decreases from 69:31 (600 °C) 39:61 (800 °C) to 19:81 (1000 °C). Table 4 shows that the catalyst alloyed at 800 °C exhibits a higher surface-specific activity compared to the 600 °C, which we attribute to a higher alloying degree and thus a higher Cu content in the core of the core-shell catalyst. We furthermore assume that for the 1000 °C sample, the activity decreases again due to the formation of a porous structure and a more severe Cu depletion of the core, as reported in literature. This however is certainly only a hypothesis that we cannot proof with our experimental methods. However, an indirect support comes from the finding, that the activity of the chemically leached samples with their porous structure found by TEM (see Fig. 4), is rather similar to the electrochemically leached sample alloyed at 1000 °C. Indeed, comparing Cu@Pt/CNTs₁₀₀₀ and the same catalyst chemically dealloyed for 1 h or 4 h (Cu@Pt/CNTs_{1h} and Cu@Pt/CNTs_{4h}), one can conclude that at least for these larger particles, chemical or electrochemical leaching have similar effects on

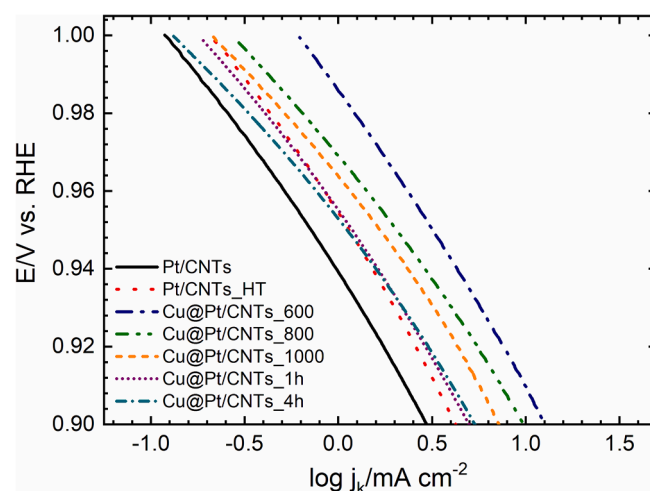


Fig. 8. Tafel plots of the different catalysts in the high-potential region. Note that the current densities are related to the geometrical area, while for Table 4 the kinetic parameters have been corrected by the catalyst mass or by the specific surface area.

activity, with surface-specific activities being between 0.321 and 0.389 mA cm^{-2} (comp. Table 4), and thus probably on structure. It is, however, intriguing that, albeit being lower than the activity of the core-shell catalysts with a Cu-rich core, in these chemically leached samples with a very low Cu content (less than 10 % of the initial one) the activity is still significantly higher than that of pure Pt, questioning the need of high Cu contents at least for porous particles. Furthermore, since all bimetallic catalysts with their likely different structure exhibit similar $Q_{\text{CO}}/2Q_{\text{H}}$ ratios in ECSA determination, we conclude that this ratio does not necessarily indicate formation of a skin around an alloy but should rather be seen as a general descriptor for a beneficial electronic structure for ORR. In a previous paper [40] a slightly better activity for the chemically leached sample was found, however with different precursor catalyst. In general, the electro/chemically dealloyed catalysts achieved specific activities between ca. 2.3 to 3.4-fold that exhibited by the pure Pt catalysts.

From a more practical point of view, the electrochemically dealloyed Cu@Pt/CNTs₆₀₀ catalyst shows ca. 3-fold mass activity compared to the pure Pt catalysts. The significant reduction in the mass activity of the catalysts annealed at temperatures higher than 600 °C is attributed to the larger particles obtained, that overcompensates any beneficial effects of the better alloying [55]. It is furthermore worth mentioning that the Tafel slopes for pure Pt and Pt-based catalysts in the high potential region are usually shown to be ca. 60 mV decade^{-1} [56], while the extracted Tafel slopes as listed in Table 4 are slightly higher. This difference has also been reported in previous literatures [57–59] and might be attributed to the potential dependence of surface adsorption [57,59].

Table 4

Kinetic parameters extracted from the ORR polarization curves: half wave potential ($E_{1/2}$), mass specific activity (MSA), surface specific activity (SSA), and Tafel slope.

Catalyst	$E_{1/2}$ V vs. RHE	MSA A/mg^{-1}		SSA mA/cm^2		Tafel slope mVdec^{-1}
		0.85 V	0.9 V	0.85 V	0.9 V	
Pt/CNTs	0.88	0.328	0.099	0.443	0.134	73
Pt/CNTs _{HT}	0.89	0.402	0.138	0.409	0.140	79
Cu@Pt/CNTs ₆₀₀	0.94	0.701	0.288	0.864	0.355	76
Cu@Pt/CNTs ₈₀₀	0.93	0.409	0.165	1.182	0.479	65
Cu@Pt/CNTs ₁₀₀₀	0.92	0.276	0.123	0.836	0.373	66
Cu@Pt/CNTs _{1h}	0.90	0.423	0.131	1.258	0.389	71
Cu@Pt/CNTs _{4h}	0.91	0.523	0.163	1.027	0.321	64

5. Conclusion

Pt nanoparticles supported onto functionalized multiwalled carbon nanotubes were prepared via microwave-assisted polyol synthesis. Heat treatment of the as-prepared Pt/CNT catalyst in ambient atmosphere at 185 °C to remove any remaining PVP traces turned out to be a beneficial step. The electrochemical characterization showed that the as-prepared Pt/CNT catalyst has lower ECSA_{Hupd} and a lower ORR activity than Pt/CNTs_{HT}. Cu@Pt/CNTs₆₀₀₋₁₀₀₀ alloy catalysts were obtained after impregnation of the former catalyst with a Cu precursor followed by a heat treatment protocol executed in H₂/Ar atmosphere, leading to an overall simple and straightforward catalyst synthesis procedure. The XRD patterns of the alloyed catalysts demonstrated an increasing degree of alloying with full alloying only at 1000 °C and at the same time significant particle growth. The initial CVs of the alloyed catalysts illustrate that these catalysts possess a Cu-rich surface however, Pt-rich surfaces were found after electro/chemical dealloying as shown by the electrochemical data. A discrepancy was found between the ECSA_{Hupd} and ECSA_{CO} of the electro/chemically dealloyed catalysts with Q_{CO}/2Q_H greater than unity while the pure Pt catalysts showed Q_{CO}/2Q_H ≈ 1, which can be explained in terms of differences in the adsorption properties between the dealloyed catalysts and Pt and also provides an indication of the formation of a Pt-rich surface. The ORR activities were investigated using the RDE technique. The electro/chemically dealloyed catalysts possess improved ORR activity relative to Pt/CNT catalysts with the electrochemically dealloyed Cu@Pt/CNTs₆₀₀ catalyst showing the highest mass specific activity and the dealloyed Cu@Pt/CNTs₈₀₀ showing the highest surface specific activity. The development of activities among the various catalysts is explained by a structural development from a core-shell arrangement of the smaller particles alloyed at lower temperatures to a more porous structure of the larger particles, may they be chemically or electrochemically leached.

CRedit authorship contribution statement

Heba El-Deeb: Conceptualization, Investigation, Formal analysis, Writing – original draft. **Abu Bakr Ahmed Amine Nassr:** Investigation. **Michael Bron:** Conceptualization, Supervision, Writing – review & editing.

Declaration of Competing Interest

The authors declare that they have no known competing financial interests or personal relationships that could have appeared to influence the work reported in this paper.

Acknowledgement

Scientific discussion with Prof. W. Grünert, Ruhr-Universität Bochum, is gratefully acknowledged

Appendix A. Supplementary data

Supplementary data to this article can be found online at <https://doi.org/10.1016/j.jelechem.2023.117724>.

References

- X.Z. Yuan, H. Wang, PEM fuel cell fundamentals, in: J. Zhang (Ed.), PEM Fuel Cell ElectroCatalysts and Catalyst Layers: Fundamentals and Applications, Springer, London, 2008, p. 25.
- W. Vielstich, A. Lamm, H.A. Gasteiger, Handbook of fuel cells: fundamentals, technology, and applications, John Wiley & Sons Ltd, Chichester, 2003.
- A. De Frank Bruijn, G.J.M. Janssen, PEM Fuel Cell Materials: Costs, Performance and Durability, 7694, in: R.A. Meyers (Ed.), Encyclopedia of Sustainability Science and Technology, Springer, New York, 2012.
- M.M. Whistona, I.L. Azevedoa, S. Litsterb, K.S. Whitefoot, C. Samarasc, J. F. Whitacre, Expert assessments of the cost and expected future performance of proton exchange membrane fuel cells for vehicles, PNAS 116 (2019) 4899.
- H.A. Gasteiger, S.S. Kocha, B. Sompalli, F.T. Wagner, Activity benchmarks and requirements for Pt, Pt-alloy, and non-Pt oxygen reduction catalysts for PEMFCs, Appl. Catal. B, Environ. 56 (2005) 9–35.
- A. Rabis, P. Rodriguez, T.J. Schmidt, Electrocatalysis for polymer electrolyte fuel cells: Recent achievements and future challenges, ACS Catal. 2 (2012) 864–890.
- M.K. Debe, Electrocatalyst approaches and challenges for automotive fuel cells, Nature 486 (2012) 43–51.
- L. Xiong, A. Manthiram, Effect of atomic ordering on the catalytic activity of carbon supported PtM (M=Fe, Co, Ni, and Cu) alloys for oxygen reduction in PEMFCs, J. Electrochem. Soc. 152 (2005) A697–A703.
- P. Mani, P.R. Srivastava, P. Strasser, Dealloyed Pt-Cu core-shell nanoparticle electrocatalysts for use in PEM fuel cell cathodes, J. Phys. Chem. C 112 (2008) 2770–2778.
- U.A. Paulus, A. Wokaun, G.G. Scherer, T.J. Schmidt, V. Stamenkovic, V. Radmilovic, N.M. Markovic, Oxygen reduction on carbon-supported Pt-Ni and Pt-Co alloy catalysts, J. Phys. Chem. B 106 (2002) 4181–4191.
- V.R. Stamenkovic, B. Fowler, B.S. Mun, G. Wang, P.N. Ross, C.A. Lucas, N. M. Markovic, Improved oxygen reduction activity on Pt₃Ni(111) via increased surface site availability, Science 315 (2007) 493–497.
- V.R. Stamenkovic, B.S. Mun, M. Arenz, K.J.J. Mayrhofer, C.A. Lucas, G. Wang, P. N. Ross, N.M. Markovic, Trends in electrocatalysis on extended and nanoscale Pt-bimetallic alloy surfaces, Nat. Mater. 6 (2007) 241–247.
- T. Bligaard, J.K. Nørskov, Ligand effects in heterogeneous catalysis and electrochemistry, Electrochim. Acta 52 (2007) 5512–5516.
- M. Oezaslan, P. Strasser, Activity of dealloyed PtCo₃ and PtCu₃ nanoparticle electrocatalyst for oxygen reduction reaction in polymer electrolyte membrane fuel cell, J. Power Sources 196 (2011) 5240–5249.
- J.X. Wang, H. Inada, L. Wu, Y. Zhu, Y. Choi, P. Liu, W. Zhou, R.R. Adzic, Oxygen reduction on well-defined core-shell nanocatalysts: Particle size, facet, and Pt shell thickness effects, J. Am. Chem. Soc. 131 (2009) 17298–17302.
- M. Oezaslan, F. Hasché, P. Strasser, Pt-based core-shell catalyst architectures for oxygen fuel cell electrodes, J. Phys. Chem. Lett. 4 (2013) 3273–3291.
- L. Gan, M. Heggen, R. O'Malley, B. Theobald, P. Strasser, Understanding and controlling nanoporosity formation for improving the stability of bimetallic fuel cell catalysts, Nano Lett. 13 (2013) 1131–1138.
- D. Wang, Y.U.H.L. Xin, R. Hovden, P. Ercius, J.A. Mundy, H. Chen, J.H. Richard, D. A. Muller, F.J. DiSalvo, H.D. Abruna, Tuning ORR activity via controllable dealloying: A model study of ordered Cu₃Pt/C intermetallic nanocatalysts, Nano Lett. 12 (2012) 5230–5238.
- J. Snyder, I. McCue, K. Livi, J. Erlebacher, Structure/Processing/Properties relationships in nanoporous nanoparticles as applied to catalysis of the cathodic oxygen reduction reaction, J. Am. Chem. Soc. 134 (2012) 8633–8645.
- M. Oezaslan, M. Heggen, P. Strasser, Size-dependent morphology of dealloyed bimetallic catalysts: Linking the nano to the macro scale, J. Am. Chem. Soc. 134 (2012) 514–524.
- N. Hodnik, M. Zorko, M. Bele, S. Hocevar, M. Gaberšček, Identical location scanning electron microscopy: A case study of electrochemical degradation of PtNi nanoparticles using a new nondestructive method, J. Phys. Chem. C 116 (2012) 21326–21333.
- P. Serp, M. Corrias, P. Kalck, Carbon nanotubes and nanofibers in catalysis, Appl. Catal. A: General 253 (2003) 337–358.
- W. Zhang, P. Sherrell, A.I. Minett, J.M. Razal, J. Chen, Carbon nanotube architectures as catalyst supports for proton exchange membrane fuel cells, Energ. Environ. Sci. 3 (2010) 1286–1293.
- H. El-Deeb, M. Bron, Microwave-assisted polyol synthesis of PtCu/carbon nanotube catalysts for electrocatalytic oxygen reduction, J. Power Sources 275 (2015) 893–900.
- H. El-Deeb, M. Bron, Electrochemical Dealloying of PtCu/CNT Electrocatalysts Synthesized by NaBH₄-Assisted Polyol-Reduction: Influence of Preparation Parameters on Oxygen Reduction Activity, Electrochim. Acta 164 (2015) 315–322.
- A modified version of this paper has been published as part of a PhD thesis: H. El-Deeb, "Synthesis and Characterization of Core-Shell Electrocatalysts for Fuel Cells Application", Halle (Germany), August 2016.
- M. Steimecke, S. Rümmler, M. Bron, The effect of rapid functionalization on the structural and electrochemical properties of high-purity carbon nanotubes, Electrochim. Acta 163 (2015) 1.
- H. Yue, Y. Zhao, X. Ma, J. Gong, Ethylene glycol: properties, synthesis, and applications, Chem. Soc. Rev. 41 (2012) 4218–4244.
- S.E. Skrabalak, B.J. Wiley, M. Kim, E.V. Formo, Y. Xia, On the polyol synthesis of silver nanostructures: glycolaldehyde as a reducing agent, Nano Lett. 8 (2008) 2077–2081.
- Z. Liu, M. Shamsuzzoha, E.T. Ada, W.M. Reichert, D.E. Nikles, Synthesis and activation of Pt nanoparticles with controlled size for fuel cell electrocatalysts, J. Power Sources 164 (2007) 472–480.
- D. Li, C. Wang, D. Tripkovic, S. Sun, N.M. Markovic, V.R. Stamenkovic, Surfactant removal for colloidal nanoparticles from solution synthesis: The effect on catalytic performance, ACS Catal. 2 (2012) 1358–1362.
- F. Habashi, S.A. Mikhail, K.V. Van, Reduction of sulfates by hydrogen, Can. J. Chem. 54 (1976) 3646.
- P.N. Nandi, D.A. Deshpande, V.G. Kher, Dehydration steps in CuSO₄•5H₂O crystals, Proc. Indian Acad. Sci. 88 (1979) 113.

- [34] S.H. Saleh, C.P. Tripp, A new approach for measuring water concentration in oil using copper sulfate powder and infrared spectroscopy, *Spectrochim. Acta A Mol. Biomol. Spectrosc.* 262 (2021), 120107.
- [35] H.A. Huy, T.V. Man, H.T. Tai, V.T.T. Ho, Preparation and characterization of high-dispersed Pt/c nano-electrocatalysts for fuel cell applications, *Vietnam J. Sci. Technol.* 54 (2016) 472–482.
- [36] D. Kim, Y. Sohn, I. Jang, S.J. Yoo, P. Kim, Formation mechanism of carbon-supported hollow PtNi nanoparticles via one-step preparations for use in the oxygen reduction reaction, *Catalysts* 12 (2022) 513.
- [37] T. Theivasanthi, M. Alagar, X-ray diffraction studies of copper nanopowder, *Arch. Phy. Res.* 1 (2010) 112–117.
- [38] J. Shanmugapriya, C.A. Reshma, V. Srinidhi, K. Harithpriya, K.M. Ramkumar, D. Umpathy, K. Gunasekaran, R. Subashini, Green synthesis of copper nanoparticles using withania somnifera and its antioxidant and antibacterial activity, *J. Nanomaterials* (2022) 7967294.
- [39] M. Oezaslan, F. Hasche, P. Strasser, In situ observation of bimetallic alloy nanoparticle formation and growth using high-temperature XRD, *Chem. Mater.* 23 (2011) 2159–2165.
- [40] O. Petrova, C. Kulp, M.M. Pohl, R. Veen, L. Veith, T. Grehl, M.W.E. van den Berg, H. Brongersma, M. Bron, W. Grünert, Chemical leaching of Pt–Cu/C catalysts for electrochemical oxygen reduction: activity, particle structure, and relation to electrochemical leaching, *ChemElectroChem* (2016) 1768–1780.
- [41] K.A. Wepasnick, B.A. Smith, J.L. Bitter, D.H. Fairbrother, Chemical and structural characterization of carbon nanotube surfaces, *Anal. Bioanal. Chem.* 396 (2010) 1003–1014.
- [42] J. Erlebacher, M.J. Aziz, A. Karma, N. Dimitrov, K. Sieradzki, Evolution of nanoporosity in dealloying, *Nature* 410 (2001) 450–453.
- [43] R.C. Newman, K. Sieradzki, *Metallic Corrosion*, Science 263 (1994) 1708–1709.
- [44] D. Wang, Y. Yu, H.L. Xin, R. Hovden, P. Ercius, J.A. Mundy, H. Chen, J.H. Richard, D.A. Muller, F.J. DiSalvo, H.D. Abruña, Tuning oxygen reduction reaction activity via controllable dealloying: A model study of ordered Cu₃Pt/C intermetallic nanocatalysts, *Nano Lett.* 12 (2012) 5230–5238.
- [45] Y.H. Chung, S.J. Kim, D.Y. Chung, H.Y. Park, Y.E. Sung, S.J. Yoo, J.H. Jang, Third-body effects of native surfactants on Pt nanoparticle electrocatalysts in proton exchange fuel cells, *Chem. Commun.* 51 (2015) 2968–2971.
- [46] I.A. Safo, C. Dosche, M. Özazlan, Effects of capping agents on the oxygen reduction reaction activity and shape stability of Pt nanocubes, *ChemPhysChem* 20 (2019) 3010–3023.
- [47] D. Zhan, J. Velmurugan, M.V. Mirkin, Adsorption/Desorption of hydrogen on Pt nanoelectrodes: evidence of surface diffusion and spillover, *J. Am. Chem. Soc.* 131 (2009) 14756–14760.
- [48] S. Rudi, C. Cui, L. Gan, P. Strasser, Comparative study of the electrocatalytically active surface areas (ECSAs) of Pt alloy nanoparticles evaluated by Hupd and CO-stripping voltammetry, *Electrocatal.* 5 (2014) 408–418.
- [49] F. Maillard, M. Eikerling, O.V. Cherstiouk, S. Schreier, E. Savinova, U. Stimming, Size effects on reactivity of Pt nanoparticles in CO monolayer oxidation: the role of surface mobility, *Faraday Discuss.* 125 (2004) 357–377.
- [50] F. Maillard, E.R. Savinova, U. Stimming, CO monolayer oxidation on Pt nanoparticles: Further insights into the particle size effects, *J. Electroanal. Chem.* 599 (2007) 221–232.
- [51] D.F.V. Vliet, C. Wang, D. Li, A.P. Paulikas, J. Greeley, R.B. Rankin, D. Strmcnik, D. Tripkovic, N.M. Markovic, V.R. Stamenkovic, Unique electrochemical adsorption properties of Pt-skin surfaces, *Angew. Chem.* 124 (2012) 3193–3196.
- [52] C. Wang, M. Chi, D. Li, D. Strmcnik, D.V. Vliet, G. Wang, V. Komanicky, K. Chang, A.P. Paulikas, D. Tripkovic, J. Pearson, K.L. More, N.M. Markovic, V. R. Stamenkovic, Design and synthesis of bimetallic electrocatalyst with multilayered Pt-skin surfaces, *J. Am. Chem. Soc.* 133 (2011) 14396–14403.
- [53] C. Wang, D.V. Vliet, K.L. More, N.J. Zaluzec, S. Peng, S. Sun, H. Daimon, G. Wang, J. Greeley, J. Pearson, A.P. Paulikas, G. Karapetrov, D. Strmcnik, N.M. Markovic, V. R. Stamenkovic, Multimetallic Au/FePt₃ nanoparticles as highly durable electrocatalyst, *Nano Lett.* 11 (2011) 919–926.
- [54] P. Strasser, S. Koh, T. Anniyev, J. Greeley, K. More, C. Yu, Z. Liu, S. Kaya, D. Nordlund, H. Ogasawara, M.F. Toney, A. Nilsson, Lattice-strain control of the activity in dealloyed core-shell fuel cell catalysts, *Nature Chem.* 2 (2010) 454–460.
- [55] S. Koh, N. Hahn, C. Yu, P. Strasser, Effects of annealing conditions on catalytic activities of Pt-Cu nanoparticle electrocatalysts for PEM Fuel Cells, *ECS Trans.* 16 (2008) 1093–1103.
- [56] S. Chen, A. Kucernak, Electrocatalysis under conditions of high mass transport rate: Oxygen reduction on single submicrometer-sized Pt particles supported on carbon, *J. Phys. Chem. B* 108 (2004) 3262–3276.
- [57] Y. Qian, W. Wen, P.A. Adcock, Z. Jiang, N. Hakim, M.S. Saha, S. Mukerjee, PtM/C catalyst prepared using reverse micelle method for oxygen reduction reaction in PEM fuel cells, *J. Phys. Chem. C* 112 (2008) 1146–1157.
- [58] H. Yang, S. Kumar, S. Zou, Electroreduction of O₂ on uniform arrays of Pt nanoparticles, *J. Electroanal. Chem.* 688 (2013) 180–188.
- [59] C. Coutanceau, M.J. Croissant, T. Napporn, C. Lamy, Electrocatalytic reduction of dioxygen at platinum particles dispersed in a polyaniline film, *Electrochim. Acta* 46 (2000) 579–588.